Source and origin of the interfacial Dzyaloshinskii-Moriya interaction in a heavy-metal|magnetic-insulator bilayer

S. Y. Xia,[1] T. Feng,[1] B. Yang,[1] G. Liu,[1] Y. Z. Tian,[1] P. Wang,[2] X. G. Wan,[1,3,*] B. G. Wang,[1,3,†] and D. Wu[1,3,‡]

[1]*National Laboratory of Solid State Microstructures, Jiangsu Provincial Key Laboratory for Nanotechnology and Department of Physics, Nanjing University, Nanjing 210093, Peoples Republic of China*

[2]*College of Mathematics and Physics and Advanced Optoelectronic Materials and Technologies Engineering Laboratory of Shandong, Qingdao University of Science and Technology, Qingdao 266061, Peoples Republic of China*

[3]*Collaborative Innovation Center of Advanced Microstructures, Nanjing University, Nanjing 210093, Peoples Republic of China*

(Received 9 November 2021; revised 8 March 2022; accepted 3 May 2022; published 16 May 2022)

The interfacial Dzyaloshinskii-Moriya interaction (iDMI) was observed in the bilayer consisting of a heavy metal and a ferromagnetic insulator such as Pt|$Tm_3Fe_5O_{12}$ (TIG), but the source and origin are still controversial. Here, we quantitatively investigate the iDMI strength in Pt|TIG by inserting a thin $Y_3Fe_5O_{12}$ layer and/or a thin Cu layer between Pt and TIG. Our results suggest the iDMI contributed by both the Pt|TIG and the TIG|substrate interfaces. At the Pt|TIG interface, we find that Pt is essential for the strong iDMI. The disentangled iDMIs for Fe-Fe and Tm-Fe pairs are comparable, revealing that the Tm ions provide not only an additional Tm-Fe iDMI, but also the spin-orbit coupling to enhance the iDMI. At the TIG|substrate interface, the iDMI is attributed to the lattice-mismatch-induced deformation of the electron cloud for the ferromagnetic ions.

DOI: 10.1103/PhysRevB.105.184417

I. INTRODUCTION

The Dzyaloshinskii-Moriya interaction (DMI) is one of the key ingredients for stabilizing nontrivial spin textures such as magnetic solitons, skyrmions, and chiral domain walls in magnetic materials [1–3], which are the promising elements for next-generation memory and logic spintronic devices [4,5]. The broken inversion symmetry together with the spin-orbit coupling (SOC) allows finite DMI to exist [6–9]. Since the inversion symmetry is broken at interfaces in multilayer films, an interfacial DMI (iDMI) is introduced [4]. This was frequently demonstrated at the interfaces between metallic ferromagnets and heavy metals (HMs), which have a large SOC to facilitate the large iDMI [10,11]. Unlike the DMI in bulk magnetic materials, which has limit approaches to be manipulated [12], the iDMI can be tuned by interfacial engineering through the stacking orders [13], the material combinations of interfaces [14,15], and external stimuli such as voltage [16,17] and current [18]. In addition, the iDMI plays an important role in the fast domain wall motion driven by either an electric current or a magnetic field [11,19–21].

In comparison to metallic ferromagnets, ferromagnetic insulators (FMIs) offer much lower damping [22], longer magnon transport length [23], and faster speed of domain wall motion [20,21]. These superior properties are attractive for magnonic and spin-wave logic devices, with the advantages of the absence of Joule heating. Very recently, observations of the topological Hall effect (THE) and the homochiral Néel domain wall in a heterostructure of a HM layer and a FMI garnet such as $Y_3Fe_5O_{12}$ (YIG) and $Tm_3Fe_5O_{12}$ (TIG) suggest the presence of the iDMI [24–28]. Such an interaction opens up a new approach to stabilize skyrmions in the FMIs and can be used to manipulate spin waves [27].

Given the importance of the iDMI in the HM|FMI bilayer, where "|" denotes the interface, it has been intensively studied to ascertain its source and origin [24,26–28]. The main difficulty in analyzing the iDMI is posed by possessing two interfaces, HM|FMI and FMI|substrate, thereby causing an active debate on the source and origin [20,24–30]. The iDMI is suggested to originate from the FMI|substrate interface based on the direct observations of skyrmions and nonreciprocal spin-wave propagation in a bare FMI-garnet film on a garnet substrate [26,27]. On the other hand, a recent study found that the THE is dramatically tuned by various metallic capping layers in the metal|TIG bilayers, strongly suggesting that the iDMI stems mainly from the metal|TIG interface [24]. In addition, as the rare-earth ion and the HM possess a strong SOC, and a Rashba SOC could be present at the oxide interface [14,28,31,32], it is still controversial regarding which one provides the required SOC [25,27,28]. Moreover, the iDMI between a pair of magnetic atoms is always accompanied by a Heisenberg exchange interaction [7,33–35]. The multiple exchange interactions between three magnetic sublattices in the rare-earth iron garnet lead to multiple pairs of the iDMI [36,37]. The disentangled iDMIs have not been investigated so far. In this work, we quantitatively investigate the iDMI in Pt|TIG|substituted-$Gd_3Ga_5O_{12}$ (SGGG) to identify the source and origin. Our results reveal that both the Pt|TIG and the TIG|SGGG interfaces have significant contributions to the iDMI. The iDMI is found to be induced by the Pt layer at the Pt|TIG interface. The disentangled iDMIs between Fe-Fe

*xgwan@nju.edu.cn
†bgwang@nju.edu.cn
‡dwu@nju.edu.cn

pairs and Tm-Fe pairs are comparable, suggesting that the Tm ions provide not only an additional Tm-Fe iDMI, but also the SOC to Tm-Fe pairs to enhance the iDMI strength significantly. We further found that the iDMI at the TIG|SGGG interface is much larger than that at the YIG|TIG interface, revealing that the large lattice mismatch leads to the iDMI at the garnet interface.

II. EXPERIMENT

The TIG and YIG films were epitaxially grown on SGGG (111) substrates by pulsed laser deposition by applying a KrF excimer laser, monitored by *in situ* reflective high-energy electron diffraction (RHEED). The target laser area was $\sim 5\,\mathrm{mm}^2$, and the target-substrate distance was 5 cm. The background pressure was 1×10^{-6} Torr. The pressure was tuned to be a dynamic pressure of 0.07 Torr by injecting pure O_2 into the chamber before heating the sample. The sample was heated by a laser with a sweeping rate of $\sim$20 K/min. After the substrates had been kept at 850 °C for 20 min, the TIG films were deposited with the laser pulses at a frequency of 2 Hz and an energy density of $\sim 5.2\,\mathrm{J/cm}^2$ on the target. The film thickness was measured by X-ray reflectivity [38], from which the growth rate was calculated to be 0.72 Å/s. The YIG films were deposited with a laser frequency of 1 Hz and an energy density of $\sim 4.5\,\mathrm{J/cm}^2$ on the target. Before the film growth on TIG|SGGG, the growth rate of YIG was measured to be 0.29 Å/s by the oscillation of the RHEED intensity [38]. Note that the TIG films of the YIG|TIG bilayers experienced an additional annealing during YIG film growth. To minimize specimen discrepancies, the single-layer TIG specimens were treated with the same thermal process as the YIG film growth. It took 30 min to turn the laser heating power gradually to zero after the film growth. Before transferring the garnet films into a magnetron sputtering chamber, the samples were ultrasonically cleaned in acetone. The metallic films were deposited by dc magnetron sputtering at room temperature. The power for both Pt and Cu is 5 W. The target-film distances for Pt and Cu are 4.1 cm and 4.3 cm, respectively. The base pressure is 8×10^{-9} Torr and the Ar pressure for sputtering is 3.8×10^{-3} Torr. The growth rates of Pt and Cu are 0.37 Å/s and 0.38 Å/s, respectively. Then the metallic films were patterned into Hall cross bars for transport measurements by optical lithography and then Ar-ion milling [38]. Transport measurements were performed in a physical property measurement system with a field sweeping rate of 1.0 mT/s [40].

Two types of the FMI-garnet films were used in this study: TIG (6.5 nm) and YIG (0.9 nm)|TIG (6.5 nm). Figure 1(a) shows the representative high-resolution X-ray diffraction (XRD) patterns of these two samples and a control YIG (9.0-nm) film. Only (444) peaks are observed for all samples, confirming the single crystalline structure and the coherent growth on the substrates [38]. The large spacing between the SGGG peak and the TIG and YIG peaks is direct evidence of the films under strong tensile strain. Owing to the small lattice difference between TIG (1.2324 nm) and YIG (1.2376 nm), the TIG peak is close to the YIG peak, resulting in a wide peak for the YIG|TIG bilayer. A flat surface with a roughness of 0.23 nm is obtained with high growth temperature and low

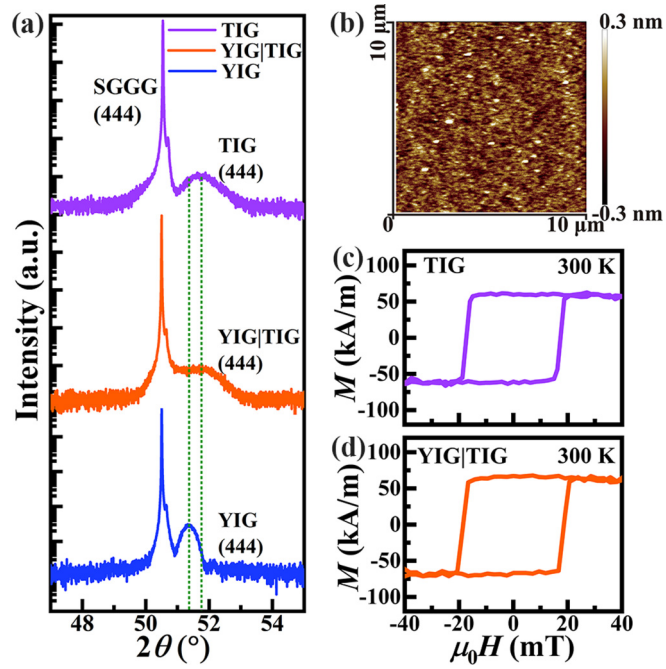

FIG. 1. (a) High-resolution XRD patterns for TIG (6.5 nm)|SGGG, YIG (0.9 nm)|TIG (6.5 nm)|SGGG, and YIG (9.0 nm)|SGGG. (b) Representative two-dimensional topography of the TIG surface characterized by AFM. The out-of-plane hysteresis loops at 300 K for (c) TIG(6.5 nm)|SGGG and (d) YIG(0.9 nm)|TIG(6.5 nm)|SGGG.

growth rate, as shown the atomic force microscopy (AFM) image in Fig. 1(b).

Figures 1(c) and 1(d) displays the out-of-plane magnetic hysteresis loops of both garnet films measured at 300 K by a superconducting quantum interference device vibrating-sample magnetometer. The loops are squared after removing the signals from the substrates, indicating strong perpendicular magnetic anisotropy (PMA). Then the 3-nm-thick Pt films were deposited on the garnet films to perform the Hall measurements. Figures 2(a) and 2(b) shows the Hall resistance (R_H), which is attributed to the spin-Hall anomalous Hall effect (SH-AHE) [41], at 300 K with the magnetic field $\mu_0 H$ perpendicular to the sample plane. The $R_H(\mu_0 H)$ curves follow very closely the magnetic hysteresis loops, implying that the R_H curves reflect the magnetic domain nucleation and magnetization switching process.

III. RESULTS AND DISCUSSION

The out-of-plane nucleation field $\mu_0 H_n$ of reversing domains in a ferromagnetic film with PMA decreases in general with increasing the in-plane field $\mu_0 H_{in}$. However, $\mu_0 H_n$ remains almost unchanged with the present iDMI below a critical $\mu_0 H_{in}$, which is closely related to the effective iDMI field $\mu_0 H_\mathrm{iDMI}$. This behavior is well described by an extended magnetic droplet nucleation model and was successfully used to determine $\mu_0 H_\mathrm{DMI}$ quantitatively from the dependence of $\mu_0 H_n$ on $\mu_0 H_{in}$ in various systems [12,42,43]. In our study, this relation is obtained by measuring R_H under an inclined field applied in the xz plane, as schematically shown in

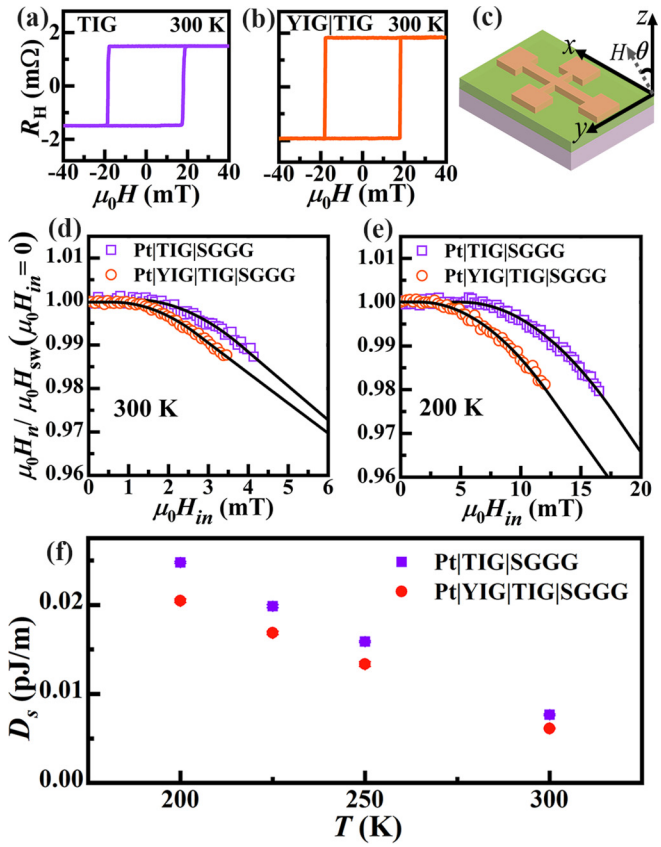

FIG. 2. The SH-AHE curves at 300 K for (a) Pt (3 nm)|TIG (6.5 nm)|SGGG and (b) Pt (3 nm)|YIG (0.9nm)|TIG (6.5 nm)|SGGG with H along the z-axis. (c) The geometry for electrical transport measurements. Normalized $\mu_0 H_n$ as a function of $\mu_0 H_{in}$ for Pt (3 nm)|TIG (6.5 nm)|SGGG and Pt (3 nm)|YIG (0.9 nm)|TIG (6.5 nm)|SGGG measured at (d) 300 K and (e) 200 K. The black curves are the fitting results based on the extended droplet model. (f) Temperature dependence of D_s for Pt|TIG|SGGG and Pt|YIG|TIG|SGGG.

Fig. 2(c), where a dc current flows along the x-axis and θ denotes the angle between the z-axis and $\mu_0 H$. $\mu_0 H_n$ and $\mu_0 H_{in}$ are calculated by $\mu_0 H_n = \mu_0 H_{sw} \cos\theta$ and $\mu_0 H_{in} = \mu_0 H_{sw} \sin\theta$, respectively, where $\mu_0 H_{sw}$ is the switching field.

Figure 2(d) presents $\mu_0 H_n$ as a function of $\mu_0 H_{in}$ for Pt|TIG|SGGG at 300 K. To determine $\mu_0 H_n$ precisely, in addition to the sharp magnetization switching, the $R_H(\mu_0 H)$ curves are averaged over substantial field scans [38]. The $\mu_0 H_n(\mu_0 H_{in})$ curve exhibits a distinct characteristic of a transition from a constant value to depending on $\mu_0 H_{in}$, in accordance with the previously described behavior, suggesting the existence of the iDMI. We further measure $\mu_0 H_n$ as a function of $\mu_0 H_{in}$ at a lower temperature, as shown in the results at 200 K in Fig. 2(e). The transition obviously occurs at higher $\mu_0 H_{in}$, indicating the iDMI enhancement. In order to ascertain the $\mu_0 H_{iDMI}$ values quantitatively, the saturation magnetization M_S, the exchange stiffness A, and the effective magnetic anisotropy K_{eff} were measured [38]. We then fit the $\mu_0 H_n(\mu_0 H_{in})$ curves using the extended magnetic droplet model with a step-by-step fitting procedure [38]. The fittings [solid black lines in Figs. 2(d) and 2(e)] are in excellent agreement with the data and yield $\mu_0 H_{iDMI}$. The iDMI energy density D is calculated by the relation $D = \mu_0 \delta M_S H_{iDMI}$, where $\delta = \sqrt{A/K_{eff}}$ is the domain wall width. To compare the iDMI between different samples, D is scaled as $D_s = Dt$ by the film thickness t. For the YIG|TIG bilayer, t is the total thickness of the bilayer. D_s monotonously increases with decreasing temperature, as shown in Fig. 2(f). D_s is smaller than our previously reported value [44], mainly because the obtained M_S and A are smaller in this study for thinner TIG film.

Because the bulk DMI cannot be present in the centrosymmetric structure of the TIG film, the observed DMI must arise from either one or both of the interfaces, Pt|TIG and TIG|SGGG, at which the inversion symmetry is broken. First, to study the Pt|TIG interface, the Tm ions are substituted with the nonmagnetic Y ions at the interface, i.e., an ultrathin YIG (0.9-nm) spacer is inserted at the Pt|TIG interface, to perform the same measurements. The measured $\mu_0 H_n$ as a function of $\mu_0 H_{in}$ at 300 K and 200 K is plotted in Figs. 2(d) and (e), respectively. The critical $\mu_0 H_{in}$ is obviously reduced in comparison with that for the Pt|TIG|SGGG sample. The reduction of the critical $\mu_0 H_{in}$ is more remarkable at low temperature. The iDMI for Pt|YIG|TIG|substrate $D_s^{Pt|YIG|TIG|sub}$ is obtained from the fitting [solid lines in Figs. 2(d) and (e)]. Figure 2(f) plots $D_s^{Pt|YIG|TIG|sub}$ at different temperatures. The iDMI decreases after removing the Tm ions at the interface, strongly suggesting that the Pt|TIG interface has contributed to the iDMI and the Tm ions play an important role. Owing to the crystalline anisotropy of the YIG and YIG|TIG films, $\mu_0 H_n$ could vary for the current flowing along different directions. However, we find that this variation is negligible [38].

Pt is generally responsible for the strong iDMI in metallic magnetic systems. To identify the role of Pt, next we insert a 1.2-nm-thick Cu layer at the interfaces to measure the iDMI. Figures 3(a) and 3(b) shows $\mu_0 H_n$ versus $\mu_0 H_{in}$ measured as in Figs. 2(d) and 2(e) for Pt|Cu|TIG|SGGG and Pt|Cu|YIG|TIG|SGGG at 300 K and 200 K, respectively. The critical $\mu_0 H_{in}$ is apparently smaller than that of the corresponding samples without the Cu spacer. Two normalized $\mu_0 H_n$ ($\mu_0 H_{in}$) curves almost overlap each other, suggesting that D_s is almost equal for Cu in contact with YIG and TIG. The fittings [solid line in Figs. 3(a) and 3(b)] reproduce the data very well. The fitted iDMI values for Pt|Cu|TIG|SGGG $D_s^{Cu|TIG|YIG|sub}$ and Pt|Cu|YIG|TIG|SGGG $D_s^{Cu|YIG|TIG|sub}$ as a function of temperature are plotted in Fig. 3(c). In comparison to the iDMI of the samples without the Cu spacer, the iDMI is significantly reduced, unambiguously indicating that the Pt layer enhances the iDMI. Moreover, the fact that the Cu spacer causes the larger reduction of the iDMI for TIG|SGGG than that for YIG|TIG|SGGG manifests again the critical role of the Tm ions on the iDMI.

We note that the temperature where D_s is extrapolated to be zero is far below the Curie temperature T_C of the magnetic layer [Figs. 2(f) and 3(c)] [38], similar to other systems [43,45,46]. The exchange interaction or magnetization is a bulk property, whereas the iDMI is a two-dimensional effect. The low dimensional effect could be more sensitive to temperature than bulk property. Therefore, it is reasonable that D_s is more sensitive to temperature than magnetization.

The iDMI is known to originate from the SOC-induced perturbations on the exchange interactions [47], but there is

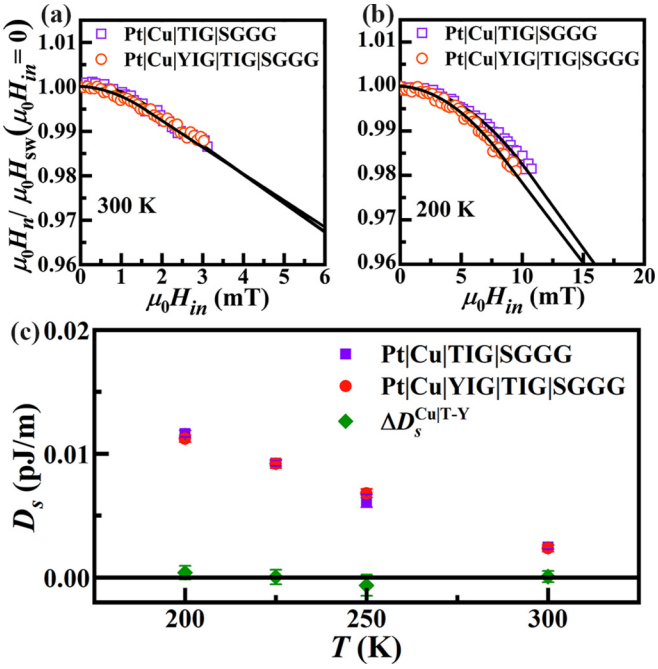

FIG. 3. Normalized $\mu_0 H_n$ as a function of $\mu_0 H_{in}$ for Pt (3 nm)|Cu (1.2 nm)|TIG (6.5 nm)|SGGG and Pt (3 nm)|Cu (1.2 nm)|YIG (0.9 nm)|TIG (6.5 nm)|SGGG measured at (a) 300 K and (b) 200 K. The black curves are the fitting results based on the extended droplet model. (c) Temperature dependence of D_s for Pt|Cu|TIG|SGGG and Pt|Cu|YIG|TIG|SGGG and $\Delta D_s^{Cu|T-Y}$.

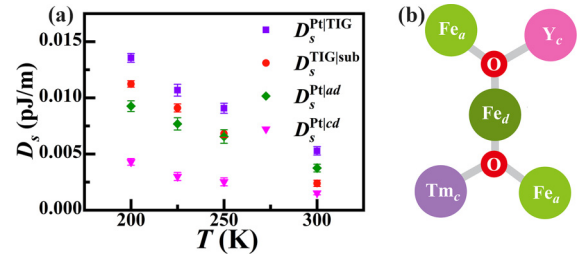

FIG. 4. (a) Temperature dependence of D_s for $D_s^{Pt|TIG}$, $D_s^{TIG|sub}$, $D_s^{Pt|ad}$, and $D_s^{Pt|cd}$ in Pt|TIG|SGGG. (b) Schematic diagram of the structural symmetry at the YIG|TIG interface for the interfacial Fe_d.

only one exchange interaction in the ferromagnet in most systems. The magnetic properties of TIG are determined by the exchange interactions between three magnetic sublattices: octahedrally coordinated Fe^{3+} (Fe_a), tetrahedrally coordinated Fe^{3+} (Fe_d), and dodecahedrally coordinated Tm^{3+} (Tm_c) [48]. Although the interaction between Fe_a and Fe_d is a strongly antiferromagnetic super-exchange (exchange constant J_{ad}), the unequal numbers of Fe_a and Fe_d per unit cell give rise to a nonzero magnetic moment. The Tm_c moment is weakly antiferromagnetically coupled to the Fe_d moment (exchange constant J_{cd}). Other exchange interactions are negligibly weak in comparison to J_{ad} and J_{cd}, meaning we only consider the iDMIs between Fe_a-Fe_d and Tm_c-Fe_d pairs. Given that the Y^{3+} ion is nonmagnetic, only the Fe_a-Fe_d interaction is considered in YIG. Therefore, the iDMIs for our four samples can be expressed as

$$D_s^{Pt|TIG|sub} = D_s^{Pt|ad} + D_s^{Pt|cd} + D_s^{TIG|sub}, \quad (1)$$

$$D_s^{Pt|YIG|TIG|sub} = D_s^{Pt|ad} + D_s^{YIG|TIG} + D_s^{TIG|sub}, \quad (2)$$

$$D_s^{Cu|TIG|sub} = D_s^{Cu|ad} + D_s^{Cu|cd} + D_s^{TIG|sub}, \quad (3)$$

and

$$D_s^{Cu|YIG|TIG|sub} = D_s^{Cu|ad} + D_s^{YIG|TIG} + D_s^{TIG|sub}, \quad (4)$$

respectively, where $D_s^{Pt|ad}$ and $D_s^{Cu|ad}$ are the Fe_a-Fe_d iDMI for Pt and Cu in contact with TIG or YIG, respectively; $D_s^{Pt|ac}$ and $D_s^{Cu|ac}$ are the Tm_c-Fe_d iDMI for Pt and Cu in contact with TIG, respectively; $D_s^{TIG|sub}$ and $D_s^{YIG|TIG}$ are the iDMIs at the TIG|SGGG and YIG|TIG interfaces, respectively.

We utilize Eqs. (1)–(4) to analyze different components in the iDMI quantitatively. Because all samples contain $D_s^{TIG|sub}$, the differences $\Delta D_s^{Pt|T-Y} \equiv D_s^{Pt|TIG|sub} - D_s^{Pt|YIG|TIG|sub} = D_s^{Pt|cd} - D_s^{YIG|TIG}$, $\Delta D_s^{Cu|T-Y} \equiv D_s^{Cu|TIG|sub} - D_s^{Cu|YIG|TIG|sub} = D_s^{Cu|cd} - D_s^{YIG|TIG}$, and $\Delta D_s^{Pt-Cu|YIG} \equiv D_s^{Pt|YIG|TIG|sub} - D_s^{Cu|YIG|TIG|sub} = D_s^{Pt|ad} - D_s^{Cu|ad}$ isolate $D_s^{TIG|sub}$. $\Delta D_s^{Cu|T-Y}$ is negligibly small within the experimental error margin for all temperatures, as shown in Fig. 3(c), i.e., $D_s^{Cu|cd} \approx D_s^{YIG|TIG}$. Accordingly, it is obtained that $\Delta D_s^{Pt|T-Y} \approx D_s^{Pt|cd} - D_s^{Cu|cd}$. It is known that the large SOC strength of the HM facilitates the iDMI strength. In comparison with Pt, the SOC strength of Cu is much weaker [49,50]. It is thus frequently found to quench the iDMI by inserting Cu between the HM and the ferromagnet [45,51]. We apply this scenario to the TIG system. Meanwhile, X-ray absorption spectroscopy reveals that the interfacial interaction at the Cu|YIG interface is much weaker than that at the Pt|YIG interface [52], meaning the influence of Cu to the local spins is much weaker than that of Pt. Therefore, we speculate $D_s^{Pt|TIG} \gg D_s^{Cu|TIG}$ or $D_s^{Pt|ad} \gg D_s^{Cu|ad}$ and $D_s^{Pt|cd} \gg D_s^{Cu|cd}$. This speculation was adopted by several reports [20,53]. With this speculation, it can be immediately estimated that $D_s^{Pt|cd} \approx \Delta D_s^{Pt|T-Y}$, $D_s^{Pt|ad} \approx \Delta D_s^{Pt-Cu|YIG}$, and $D_s^{Cu|cd} \approx D_s^{YIG|TIG} \approx 0$. We can then calculate $D_s^{TIG|sub} \approx D_s^{Cu|YIG|TIG|sub}$, and the iDMI at the Pt|TIG interface $D_s^{Pt|TIG} = D_s^{Pt|TIG|sub} - D_s^{TIG|sub}$. The obtained temperature dependences of $D_s^{Pt|TIG}$, $D_s^{TIG|sub}$, $D_s^{Pt|ad}$, and $D_s^{Pt|cd}$ are plotted in Fig. 4(a). Clearly, both the Pt|TIG and the TIG|SGGG interfaces have significant contributions to the iDMI.

The iDMI strength is generally proportional to the exchange interaction constant [7,33,34]. If only the Pt layer provides the SOC to the Fe_a-Fe_d and Tm_c-Fe_d pairs at the Pt|TIG interface, $D_s^{Pt|ad}$ is expected to be much larger than $D_s^{Pt|cd}$ because J_{ad} is one order of magnitude larger than J_{cd} [54]. However, $D_s^{Pt|ad}$ is only about twice as large as $D_s^{Pt|cd}$. In addition to Pt, the SOC of the rare-earth Tm ions in the TIG film itself could be also responsible for the iDMI. Since the $4f$-electrons of the Tm ions are considerably localized, the SOC of Tm has influence only on the Tm_c-Fe_d pairs and thereby $D_s^{Pt|cd}$, leading to the substantial enhancement of $D_s^{Pt|cd}$. Therefore, the Tm ions introduced in TIG not only add a pair of the exchange interaction and the corresponding

iDMI, but also provide the SOC to the Tm_c-Fe_d iDMI, resulting in the significant iDMI enhancement.

We find $D_s^{TIG|sub} \gg D_s^{YIG|TIG} \approx 0$ for the YIG|TIG and TIG|SGGG interfaces. In the HM|ferromagnet heterostructures, the iDMI emerges due to the strong SOC provided by the HM and the broken inversion symmetry at the interface, which induces the spatial deformation of the electron cloud for the ferromagnetic atoms. On the other hand, the iDMI induced by the light elements such as graphene and hydrogen is attributed to the deformation of the electron cloud resulting from the interfacial orbital hybridization [32,55,56], accompanied by the presence of the required Rashba SOC for the iDMI. This scenario could be applied to the insulator interface. At the YIG|TIG interface, the Fe_a and Fe_d sublattices are continuous across the interface, but the Tm_c sublattice is discontinuous. Given that the dominant interactions are between the Y_c-Fe_d, Tm_c-Fe_d, and Fe_a–Fe_d pairs, only the electron cloud of the interfacial Fe_d ions could be deformed due to the asymmetric interaction from Y_c and Tm_c, as schematically shown in Fig. 4(b) (see the Supplemental Material for other magnetic ions [38]). The interaction strength between the rare-earth ion and the neighboring ion via oxygen depends on the radius of the ion, the bond angle, and the bond distance. There is little difference in the radius between the Y^{3+} (1.06 Å) and Tm^{3+} ions (1.04 Å) [48]. Owing to the similar lattice constants of YIG and TIG, the YIG and TIG films epitaxially grown on SGGG have similar distortion, indicating that the bond angle and bond distance remain almost unchanged across the interface. As a result, the interaction strengths of the Y_c-Fe_d and Tm_c-Fe_d pairs are almost identical, meaning the negligible deformation of the electron cloud for the interfacial Fe_d ions and thereby the negligible Rashba SOC and iDMI. In sharp contrast, across the TIG|SGGG interface, not only the Tm_c, Fe_c, and Fe_d sublattices are discontinuous, but also the bond angle and bond distance have significant changes due to the large lattice mismatch between TIG and SGGG [Fig. 1(a)]. As a result, the electron cloud of the interfacial Tm_c, Fe_a, and Fe_d ions is remarkably deformed, leading to a finite Rashba SOC and iDMI.

IV. CONCLUSION

In conclusion, we measured D_s in Pt|TIG|SGGG and the samples with inserting Cu or/and YIG between Pt and TIG based on the magnetic extended droplet model. The obviously reduced D_s with the Cu and the YIG spacers unambiguously suggests the essential role of the Pt layer and the Tm ions. D_s at two interfaces is extracted by comparing D_s of different samples. We find that D_s at the Pt|TIG interface is comparable with that at the TIG|substrate interface. Although the exchange interaction between the Tm_c-Fe_d pair is much weaker than that between the Fe_a-Fe_d pair, the estimated D_s for these two pairs is comparable, revealing that the Tm ions provide both an additional Tm_c-Fe_d iDMI and the SOC to the Tm_c-Fe_d pair to enhance the iDMI significantly. The iDMI at the TIG|substrate interface is induced by the large lattice mismatch between the epitaxial FMI film and the substrate [28]. These findings pave the way for fine-tuning the iDMI in the FMIs.

ACKNOWLEDGMENTS

This work was supported by the National Key R&D Program of China (Grant No. 2017YFA0303202) and the National Natural Science Foundation of China (Grants No. 52025012 and No. 11727808).

[1] S. Pizzini, J. Vogel, S. Rohart, L. D. Buda-Prejbeanu, E. Jué, O. Boulle, I. M. Miron, C. K. Safeer, S. Auffret, G. Gaudin, and A. Thiaville, Chirality-Induced Asymmetric Magnetic Nucleation in Pt/Co/AlO*x* Ultrathin Microstructures, Phys. Rev. Lett. **113**, 047203 (2014).

[2] M. J. Benitez, A. Hrabec, A. P. Mihai, T. A. Moore, G. Burnell, D. McGrouther, C. H. Marrows, and S. McVitie, Magnetic microscopy and topological stability of homochiral Néel domain walls in a Pt/Co/AlO*x* trilayer, Nat. Commun. **6**, 8957 (2015).

[3] Y. Yoshimura, K. J. Kim, T. Taniguchi, T. Tono, K. Ueda, R. Hiramatsu, T. Moriyama, K. Yamada, Y. Nakatani, and T. Ono, Soliton-like magnetic domain wall motion induced by the interfacial Dzyaloshinskii–Moriya interaction, Nat. Phys. **12**, 157 (2016).

[4] A. Fert, V. Cros, and J. Sampaio, Skyrmions on the track, Nat. Nanotech. **8**, 152 (2013).

[5] L. Caretta, M. Mann, F. Büttner, K. Ueda, B. Pfau, C. M. Günther, P. Hessing, A. Churikova, C. Klose, M. Schneider, D. Engel, C. Marcus, D. Bono, K. Bagschik, S. Eisebitt, and G. S. D. Beach, Fast current-driven domain walls and small skyrmions in a compensated ferrimagnet, Nat. Nanotech. **13**, 1154 (2018).

[6] I. E. Dzialoshinskii, Thermodynamic theory of "weak" ferromagnetism in antiferromagnetic substances, Sov. Phys. JETP **5**, 1259 (1957).

[7] T. Moriya, Anisotropic superexchange interaction and weak ferromagnetism, Phys. Rev. **120**, 91 (1960).

[8] A. Fert and P. M. Levy, Role of Anisotropic Exchange Interactions in Determining the Properties of Spin-Glasses, Phys. Rev. Lett. **44**, 1538 (1980).

[9] M. Bodel, M. Heide, K. V. Bergmann, P. Ferriani, S. Heinze, G. Bihlmayer, A. Kubetzka, O. Pietzsch, S. Blüge, and R. Wiesendanger, Chiral magnetic order at surfaces driven by inversion asymmetry, Nature (London) **447**, 190 (2007).

[10] V. Kashid, T. Schena, B. Zimmermann, Y. Mokrousov, S. Blügel, Vaishali Shah, and H. G. Salunke, Dzyaloshinskii-Moriya interaction and chiral magnetism in 3d-5d zigzag chains: Tight-binding model and *ab initio* calculations, Phys. Rev. B **90**, 054412 (2014).

[11] J. Torrejon, J. Kim, J. Sinha, S. Mitani, M. Hayashi, M. Yamanouchi, and H. Ohno, Interface control of the magnetic chirality in CoFeB/MgO heterostructures with heavy-metal underlayers, Nat. Commun. **5**, 4655 (2014).

[12] D. H. Kim, M. Haruta, H. W. Ko, G. Go, H. J. Park, T. Nishimura, D. Y. Kim, T. Okuno, Y. Hirata, Y. Futakawa, H. Yoshikawa, W. Ham, S. Kim, H. Kurata, A. Tsukamoto, Y. Shiota, T. Moriyama, S. B. Choe, K. J. Lee, and T. Ono, Bulk Dzyaloshinskii–Moriya interaction in amorphous ferrimagnetic alloys, Nat. Mater. **18**, 685 (2019).

[13] J. Y. Chauleau, W. Legrand, N. Reyren, D. Maccariello, S. Collin, H. Popescu, K. Bouzehouane, V. Cros, N. Jaouen, and A. Fert, Chirality in Magnetic Multilayers Probed by the Symmetry and the Amplitude of Dichroism in X-Ray Resonant Magnetic Scattering, Phys. Rev. Lett. **120**, 037202 (2018).

[14] A. Soumyanarayanan, M. Raju, A. L. G. Oyarce, A. K. C. Tan, M. Y. Im, A. P. Petrovic, P. Ho, K. H. Khoo, M. Tran, C. K. Gan, F. Ernult, and C. Panagopoulos, Tunable room-temperature magnetic skyrmions in Ir/Fe/Co/Pt multilayers, Nat. Mater. **16**, 898 (2017).

[15] S. Banerjee, O. Erten, and M. Randeria, Ferromagnetic exchange, spin-orbit coupling and spiral magnetism at the $LaAlO_3/SrTiO_3$ interface, Nat. Phys. **9**, 626 (2013).

[16] T. Koyama, Y. Nakatani, J. Ieda, and D. Chiba, Electric field control of magnetic domain wall motion via modulation of the Dzyaloshinskii-Moriya interaction, Sci. Adv. **4**, eaav0265 (2018).

[17] L. Wang, Q. Feng, Y. Kim, R. Kim, K. H. Lee, S. D. Pollard, Y. J. Shin, H. Zhou, W. Peng, D. Lee, W. Meng, H. Yang, J. H. Han, M. Kim, Q. Lu, and T. W. Noh, Ferroelectrically tunable magnetic skyrmions in ultrathin oxide heterostructures, Nat. Mater. **17**, 1087 (2018).

[18] N. Kato, Ma. Kawaguchi, Y. C. Lau, T. Kikuchi, Y. Nakatani, and M. Hayashi, Current-Induced Modulation of the Interfacial Dzyaloshinskii-Moriya Interaction, Phys. Rev. Lett. **122**, 257205 (2019).

[19] K. S. Ryu, S. H. Yang, L. Thomas, and S. Parkin, Chiral spin torque at magnetic domain walls, Nat. Nanotech. **8**, 527 (2013).

[20] C. O. Avci, E. Rosenberg, L. Caretta, F. Buttner, M. Mann, C. Marcus, D. Bono, C. A. Ross, and G. S. D. Beach, Interface-driven chiral magnetism and current-driven domain walls in insulating magnetic garnets, Nat. Nanotech. **14**, 561 (2019).

[21] S. Emori, U. Bauer, S. M. Ahn, E. Martinez, and G. S. D. Beach, Current-driven dynamics of chiral ferromagnetic domain walls, Nat. Mater. **12**, 611 (2013).

[22] A. Franson, N. Zhu, S. Kurfman, M. Chilcote, D. R. Candido, K. S. Buchanan, M. E. Flatté, H. X. Tang, and E. J. Halperin, Low-damping ferromagnetic resonance in electron-beam patterned, high-Q vanadium tetracyanoethylene magnon cavities, APL Mater. **7**, 121113 (2019).

[23] L. J. Cornelissen, J. Liu, R. A. Duine, J. B. Youssef, and B. J. Van Wees, Long-distance transport of magnon spin information in a magnetic insulator at room temperature, Nat. Phys. **11**, 1022 (2015).

[24] A. J. Lee, A. S. Ahmed, J. Flores, S. Guo, B. Wang, N. Bagués, D. W. McComb, and F. Yang, Probing the Source of the Interfacial Dzyaloshinskii-Moriya Interaction Responsible for the Topological Hall Effect in Metal/Tm_3Fe_5O systems, Phys. Rev. Lett. **124**, 107201 (2020).

[25] A. J. Lee, S. Guo, J. Flores, B. Wang, N. Bagués, D. W. McComb, and F. Yang, Investigation of the role of rare-earth elements in spin-Hall topological Hall effect in Pt/ferrimagnetic-garnet bilayers, Nano Lett. **20**, 4667 (2020).

[26] S. Ding, A. Ross, R. Lebrun, S. Becker, K. Lee, I. Boventer, S. Das, Y. Kurokawa, S. Gupta, J. Yang, G. Jakob, and M. Kläui, Interfacial Dzyaloshinskii-Moriya interaction and chiral magnetic textures in a ferrimagnetic insulator, Phys. Rev. B **100**, 100406(R) (2019).

[27] H. Wang, J. Chen, T. Liu, J. Zhang, K. Baumgaertl, C. Guo, Y. Li, C. Liu, P. Che, S. Tu, S. Liu, P. Gao, X. Han, D. Yu, M. Wu, D. Grundler, and H. Yu, Chiral Spin-Wave Velocities Induced by All-Garnet Interfacial Dzyaloshinskii-Moriya Interaction in Ultrathin Yttrium Iron Garnet Films, Phys. Rev. Lett. **124**, 027203 (2020).

[28] L. Caretta, E. Rosenberg, F. Büttner, T. Fakhrul, P. Gargiani, M. Valvidares, Z. Chen, P. Reddy, D. A. Muller, C. A. Ross, and G. S. D. Beach, Interfacial Dzyaloshinskii-Moriya interaction arising from rare-earth orbital magnetism in insulating magnetic oxides, Nat. Commun. **11**, 1090 (2020).

[29] Q. Shao, Y. Liu, G. Yu, S. K. Kim, X. Che, C. Tang, Q. L. He, Y. Tserkovnyak, J. Shi, and K. L. Wang, Topological Hall effect at above room temperature in heterostructures composed of a magnetic insulator and a heavy metal, Nat. Electron. **2**, 182 (2019).

[30] R. Schlitz, S. Vélez, A. Kamra, C. H. Lambert, M. Lammel, S. T. B. Goennenwein, and P. Gambardella, Control of Nonlocal Magnon Spin Transport Via Magnon Drift Currents, Phys. Rev. Lett. **126**, 257201 (2021).

[31] A. D. Caviglia, M. Gabay, S. Gariglio, N. Reyren, C. Cancellieri, and J. M. Triscone, Tunable Rashba Spin-Orbit Interaction at Oxide Interfaces, Phys. Rev. Lett. **104**, 126803 (2010).

[32] H. Yang, G. Chen, A. A. C. Cotta, A. T. N'Diaye, S. A. Nikolaev, E. A. Soares, W. A. A. Macedo, K. Liu, A. K. Schmid, A. Fert, and M. Chshiev, Significant Dzyaloshinskii–Moriya interaction at graphene–ferromagnet interfaces due to the Rashba effect, Nat. Mater. **17**, 605 (2018).

[33] Y. Zhou, R. Mansell, S. Valencia, F. Kronast, and S. Van Dijken, Temperature dependence of the Dzyaloshinskii-Moriya interaction in ultrathin films, Phys. Rev. B **101**, 054433 (2020).

[34] H. T. Nembach, J. M. Shaw, M. Weiler, E. Jué, and T. J. Silva, Linear relation between Heisenberg exchange and interfacial Dzyaloshinskii–Moriya interaction in metal films, Nat. Phys. **11**, 825 (2015).

[35] A. McDannald, L. Kuna, M. S. Seehra, and M. Jain, Magnetic exchange interactions of rare-earth-substituted DyCrO3 bulk powders, Phys. Rev. B **91**, 224415 (2015).

[36] T. Bayaraa, C. Xu, D. Campbell, and L. Bellaiche, Tuning magnetization compensation and Curie temperatures in epitaxial rare earth iron garnet films, Phys. Rev. B **100**, 214412 (2019).

[37] R. Nakamoto, B. Xu, C. Xu, H. Xu, and L. Bellaiche, Properties of rare-earth iron garnets from first principles, Phys. Rev. B **95**, 024434 (2017).

[38] See Supplemental Material at http://link.aps.org/supplemental/10.1103/PhysRevB.105.184417 for growth of the TIG and YIG films, measurements of the nucleation field, saturation magnetization, exchange stiffness, and effective magnetic anisotropy of the TIG and YIG|TIG films; procedure for the fittings and fitting parameters; and interaction of the interfacial magnetic ions at the YIG|TIG interface, which includes Refs. [39,40].

[39] Q. Shao *et al.*, Role of dimensional crossover on spin-orbit torque efficiency in magnetic insulator thin films, Nat. Commun. **9**, 3612 (2018).

[40] D. Lau, V. Sundar, J.-G. Zhu, and V. Sokalski, Energetic molding of chiral magnetic bubbles, Phys. Rev. B **94**, 060401(R) (2016).

[41] C. Tang, P. Sellappan, Y. Liu, Y. Xu, J. E. Garay, and J. Shi, Anomalous Hall hysteresis in $Tm_3Fe_5O_{12}$/Pt with strain-induced perpendicular magnetic anisotropy, Phys. Rev. B **94**, 140403(R) (2016).

[42] S. Kim, P.-H. Jang, D.-H. Kim, M. Ishibashi, T. Taniguchi, T. Moriyama, K. J. Kim, K. J. Lee, and T. Ono, Magnetic droplet nucleation with a homochiral Néel domain wall, Phys. Rev. B **95**, 220402(R) (2017).

[43] S. Kim, K. Ueda, G. Go, P. H. Jang, K. J. Lee, A. Belabbes, A. Manchon, M. Suzuki, Y. Kotani, T. Nakamura, K. Nakamura, T. Koyama, D. Chiba, K. T. Yamada, D. H. Kim, T. Moriyama, K. J. Kim, and T. Ono, Correlation of the Dzyaloshinskii–Moriya interaction with Heisenberg exchange and orbital asphericity, Nat. Commun. **9**, 1648 (2018).

[44] S. Xia, S. Zhang, Z. Luan, L. Zhou, J. Liang, G. Liu, B. Yang, H. Yang, R. Liu, and D. Wu, Interfacial Dzyaloshinskii-Moriya interaction between ferromagnetic insulator and heavy metal, Appl. Phys. Lett. **116**, 052404 (2020).

[45] S. Schlotter, P. Agrawal, and G. S. D. Beach, Temperature dependence of the Dzyaloshinskii-Moriya interaction in Pt/Co/Cu thin film heterostructures, Appl. Phys. Lett. **113**, 092402 (2018).

[46] Y. Zhang, X. Kong, G. Xu, Y. Jin, C. Jiang, and G. Chai, Direct observation of the temperature dependence of the Dzyaloshinskii–Moriya interaction, J. Phys. D Appl. Phys. **55**, 195304 (2022).

[47] M. Kuepferling, A. Casiraghi, G. Soares, G. Durin, F. Garcia-Sanchez, L. Chen, C. H. Back, C. H. Marrows, S. Tacchi, and G. Carlotti, Measuring interfacial Dzyaloshinskii-Moriya interaction in ultra-thin magnetic films, arXiv:2009.11830.

[48] L. Néel, R. Pauthenet, and B. Dreyfus, Chapter VII the rare earth garnets, Prog. Low Temp. Phys. **4(C)**, 344 (1964).

[49] A. Yagmur, S. Karube, K. Uchida, K. Kondou, R. Iguchi, T. Kikkawa, Y. Otani, and E. Saitoh, Spin-current-driven thermoelectric generation based on interfacial spin-orbit coupling, Appl. Phys. Lett. **108**, 242409 (2016).

[50] L. Zhou, H. Song, K. Liu, Z. Luan, P. Wang, L. Sun, S. Jiang, H. Xiang, Y. Chen, J. Du, H. Ding, K. Xia, J. Xiao, and D. Wu, Observation of spin-orbit magnetoresistance in metallic thin films on magnetic insulators, Sci. Adv. **4**, eaao3318 (2018).

[51] H. T. Nembach, E. Jué, E. R. Evarts, and J. M. Shaw, Correlation between Dzyaloshinskii-Moriya interaction and orbital angular momentum at an oxide-ferromagnet interface, Phys. Rev. B **101**, 020409(R) (2020).

[52] P. Wang, H. Zhao, S. Liu, Y. Y. Chin, H. J. Lin, B. M. Zhang, Z. Yuan, S. W. Jiang, H. F. Ding, J. Du, Q. Y. Xu, K. Xia, and D. Wu, Reduced interfacial magnetic moment of $Y_3Fe_5O_{12}$ by capping Pt, Appl. Phys. Lett. **113**, 182402 (2018).

[53] S. Ding, L. Baldrati, A. Ross, Z. Ren, R. Wu, S. Becker, G. Jakob J. Yang, A. Brataas, and M. Kläui, Identifying the origin of the nonmonotonic thickness dependence of spin-orbit torque and interfacial Dzyaloshinskii-Moriya interaction in a ferrimagnetic insulator heterostructure, Phys. Rev. B **102**, 054425 (2020).

[54] D. Campbell, C. Xu, T. Bayaraa, and L. Bellaiche, Finite-temperature properties of rare-earth iron garnets in a magnetic field, Phys. Rev. B **102**, 144406 (2020).

[55] G. Chen, M. Robertson, M. Hoffmann, C. Ophus, A. L. F. Cauduro, R. L. Conte, H. Ding, R. Wiesendanger, S. Blügel, A. K. Schmid, and K. Liu, Observation of Hydrogen-Induced Dzyaloshinskii-Moriya Interaction and Reversible Switching of Magnetic Chirality, Phys. Rev. X **11**, 021015 (2021).

[56] G. Chen, A. Mascaraque, H. Jia, B. Zimmermann, M. Robertson, R. L. Conte, M. Hoffmann, M. A. G. Barrio, H. Ding, R. Wiesendanger, E. G. Michel, S. Blügel, A. K. Schmid, and K. Liu, Large Dzyaloshinskii-Moriya interaction induced by chemisorbed oxygen on a ferromagnet surface, Sci. Adv. **6**, eaba4924 (2020).